Friction stir processing of newly-designed Mg-5Al-3.5Ca-1Mn (AXM541) alloy: microstructure evolution and mechanical properties

S.S. Nene[a], S. Zellner[a], B. Mondal[a], M. Komarasamy[a], R.S. Mishra[a*], R.E. Brennan[b], K.C. Cho[b]

[a]*Center for Friction Stir Processing, Department of Materials Science and Engineering, University of North Texas, Denton, Texas 76207 USA*

[b]*Weapons and Materials Research Directorate, U.S. Army Research Laboratory, Aberdeen Proving Grounds, MD 21005 USA*

**Corresponding author: Rajiv.Mishra@unt.edu*

Abstract

Friction stir processing (FSP) of a new rare earth-free Mg-5Al-3.5Ca-1Mn (AXM541) alloy resulted in significant microstructural refinement and mechanical properties comparable to existing AXM series Mg alloys. Severe refinement of the Al-Ca (C36) phase during FSP led to uniform dispersion throughout the microstructure. The synergistic effect of high heat input and the presence of these 1-4 µm size particles resulted in dynamic recrystallization via particle stimulated nucleation (PSN), with an average grain size of 4.5 µm after FSP. Further, improved mechanical properties of the AXM541 alloy along the processing direction produced a tensile yield strength (TYS) of 322 ± 14 MPa and a total elongation of 16 ± 3%. The increase in strength was also attributed to the dispersion strengthening effect associated with Al-Ca and Al-Mn (D810) particles. Moreover, the AXM541 alloy showed a better mechanical response compared with other AXM alloys irrespective of high Ca/Al ratio, due to the effective refinement and redistribution of Al-Ca phases resulting from FSP. However, strain hardening ability and TYS of the AXM541 alloy could be further improved if the Mn/Al ratio could be tailored, as Al-Mn particles do not break down during FSP.

Keywords: Magnesium alloys; strength; ductility; friction stir processing; alloy design

1. Introduction

The good strength-to-weight ratio of Mg (and its alloys) makes it especially attractive for automotive applications, as vehicle fuel consumption is greatly reduced. Recently, Mg and its alloys have been used to produce powertrains in die cast form. However, their limited use in

wrought form for similar applications is attributed to low strength, limited formability, and poor corrosion resistance [1-4]. Similarly, recent efforts to obtain ultrahigh strength and corrosion-resistant Mg alloys (with strengths as high as 400 MPa) by adding high concentrations of rare earth (RE) elements such as Y, Gd, and Zr also make the alloys extremely costly [1-4].

Other commercial Mg alloys (e.g., Mg-Al, Mg-Zn and Mg-Al-Zn alloys) have shown strength comparable to 6000 and 7000 series Al alloys, but only through the use of severe plastic deformation processes such as equal channel angular pressing (ECAP) and torsion. These processes are cost-inefficient and not industrially feasible [5-8]. Recent work on wrought Mg alloy systems such as Mg-Zn-Ca, Mg-Zn-Ag-Ca-Zr, Mg-Sn-Zn-Al has confirmed that high strengths can be obtained by normal extrusion and precipitation hardening, but at the expense of poor ductility [8-9].

In short, research geared towards the realization of new RE-free wrought Mg alloys that have significant strength and ductility combinations is necessary. Indeed, efforts have been directed to Mg-Al-Ca based alloys with good potential for attaining significant property profiles at lower costs [5-8]. This advancement has been attributed mainly to the presence of thermally stable intermetallic compounds as a part of the eutectic. Such compounds include Mg_2Ca (C14), $(Mg,Al)_2$ Ca (C36) and Al_2Ca (C15), depending on the Ca/Al ratio in the microstructure [9]. By increasing the Ca/Al ratio, the phases have followed the sequence of Al_2Ca-$(Mg,Al)_2$ Ca-Mg_2Ca forming as a part of the eutectic. Further, Li et al. [9] investigated systematically the effect of Ca/Al on the formation of these phases. They observed that a higher Ca/Al ratio of about 0.9-1.5 resulted in the formation of Mg_2Ca, whereas a ratio of 0.25-0.5 resulted in the formation of Al_2Ca as a part of the eutectic. Intermediate values of 0.5-0.9 led to C36 phase formation in the microstructure [9-13]. In addition to the phases mentioned above for Mg-Al-Ca alloys, Mn has been an inherent part of the composition, and has led to the formation of a D810 phase (popularly known as the Al_8Mn_5 phase) in Mg-Al-Ca-Mn (AXM) alloys, depending on Ca/Al and Mn/Al ratios, respectively [7-13].

Researchers have established that these Al-Ca- and Al-Mn-rich phases are important in microstructural engineering for achieving the desired combination of properties in AXM series alloys during extrusion [6-13]. Thus, the present study has focused on designing a new composition of an Mg-Al-Ca-Mn alloy and evaluating its mechanical properties after obtaining wrought microstructures through friction stir processing (FSP). A brief study focused on how Al-

Ca and Al-Mn phases affect microstructure refinement and the resultant mechanical properties for an Mg-4Al-3.5Ca-1Mn (all in weight %) alloy after FSP.

2. Experimental

Mg-Al-Ca-Mn alloy design was accomplished using Thermo-Calc software to predict its composition and phases. The alloy was obtained in cast condition in the form of a billet. The as-received nominal composition of the new Mg-4Al-3.5Ca-1Mn alloy (henceforth designated as AXM541) is given in Table 1. A flat 13 mm-thick plate was cut from the billet and friction stir processed at a rotational speed of 500 RPM, a transverse speed of 2 ipm, and at a tilt of 0.5º. The processing tool was 18 mm in diameter with a concave pin length of 5.7 mm and a diameter of 6 mm. Metallographic samples were prepared by polishing to 0.05 µm using diamond paste, followed by etching with an acetic picral solution. The microstructure was characterized along the cross section using a Nova Nano Scanning Electron Microscopy (SEM) with an Electron Dispersive Spectroscopy (EDS) attachment. Phases were identified using EDS and X-ray diffraction (XRD) analysis. Hardness was measured on a microhardness testing machine in the nugget region (from top to bottom). Room temperature tensile tests were carried out on samples of 2 mm gauge length at an initial strain rate of 1×10^{-3} s^{-1}.

Table 1: Nominal alloy composition of AXM541 alloy (all in weight %)

Condition	Mg	Al	Ca	Mn
As-cast	Balance	3.85	3.12	0.95

3. Results

3.1 Design approach and phase analysis for Mg-5Al-3.5Ca-1Mn (AXM541) alloy

As mentioned in section 1, the main concern in Mg alloys is their limited plasticity, which is attributed to the fewer slip systems available at room temperature. Extensive work to overcome this drawback has focused on alloying additions to pure Mg, which set the foundation for the design of AZ series Mg alloys. The main strategy behind adding Al to Mg is to change the c/a ratio as well as to form an intermetallic compound that assists in randomizing the preferential nucleation of grains (i.e., their texture). Although AZ series alloys display higher strength than pure Mg, these alloys still exhibit poor formability because of the presence of a brittle $Mg_{17}Al_{12}$ phase in the microstructure [2]. Hence, further attempts by researchers to add RE elements to Mg

gave rise to exceptionally higher strengths but with associated high alloying costs. Thus, the recent trend is to design Mg alloys with cost-effective alloying additions such as Al, Ca, Li, Mn and Zn, to provide balance between enhanced properties and cost; this approach offers a strong path for further research [4-15].

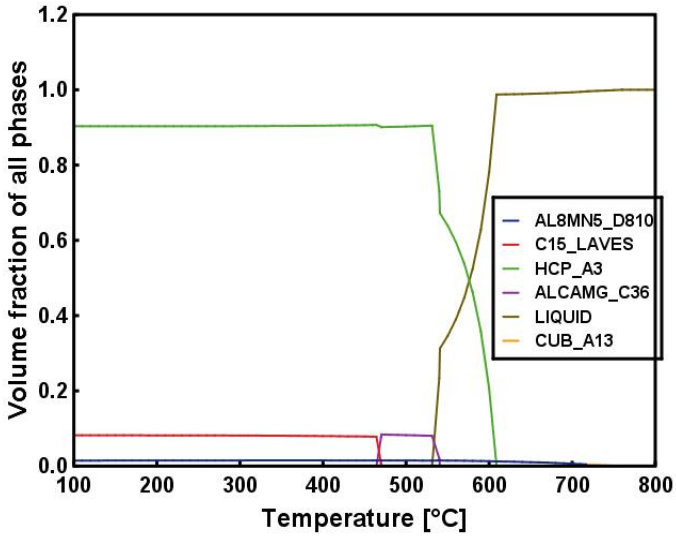

Figure 1. Phase diagram for Mg-4Al-3.5Ca-1Mn alloy (AXM541) using Thermocalc software.

The present work considers Al, Ca and Mn as alloying additions based on the expectation of enhanced microstructural efficiency [16]. The amounts of these elements were deduced from thermodynamic simulations using Thermo-Calc software, which predicted the type of phases that may form in the microstructure. As the aim was to refine the as-cast microstructure of the new alloy by FSP, which uses severe deformation and heat in synergy, second-phase particles that can be either dissolved or refined are expected to promote attaining the maximum benefit. As mentioned earlier, a Ca/Al ratio > 0.9 led to the formation of an Mg_2Ca phase that is extremely brittle. So, the Ca/Al ratio was chosen to be 0.7, such that it will form a more soluble C36 phase. Also, the amount of Mn was fixed based on thermodynamic calculations that showed the formation of a D810 phase in the matrix at 1 wt%. Hence, alloy composition was fixed to Mg-4Al-3.5Ca-1Mn, and the probable phases in the microstructure for this composition were predicted from the Thermo-Calc phase diagram (Figure 1).

The Thermo-Calc phase diagram of the AXM alloy (Figure 1) predicted the formation of α-Mg, C36, D810 and C15 phases in the microstructure when the composition was selected as Mg-

5Al-3.5Ca-1Mn (all in wt%). Secondary electron images of the AXM541 alloy in the as-cast condition (Figure 2 (a)) showed the presence of a pro-eutectic α-Mg phase (A13), along with a eutectic consisting of α-Mg + $(Al, Mg)_2Ca$ (C36) phases, both in lamellar and divorced morphologies. The presence of these phases was further confirmed by XRD analysis (Figure 2 (b)) showing pronounced peaks for the α-Mg phase as well as intense peaks for the C36 and D810 phases (enlarged inset in Figure 2 (b)). High magnification imaging of the eutectic clearly displayed the lamellar C36 phase (Figure 2 (c)) and the partially divorced eutectic region in the microstructure. Further, Mn was observed in the form of an Al_8Mn_5 phase (D810) (Figure 2 (d)) and confirmed using EDS point analysis (Figure 2 (a)), which revealed the presence of Mn-rich regions.

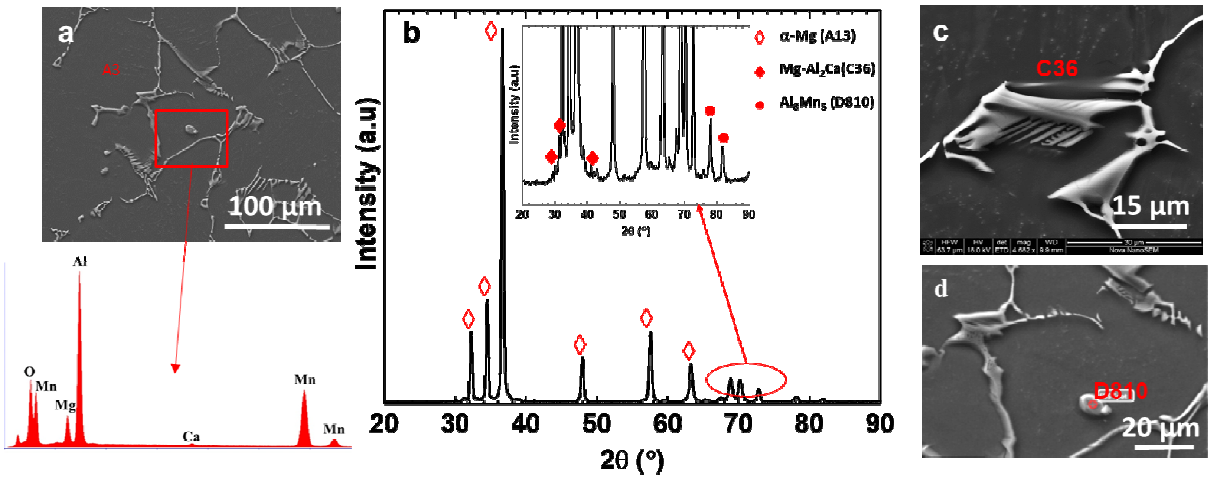

Figure 2. Microstructure of as-received AXM541 alloy showing (a) the presence of pro-eutectic α-Mg (A13) and eutectic (A13+C36 phase), (b) XRD analysis showing the presence for $(Mg, Al)_2Ca$, A13, C36 and D810 phases in as-cast condition (c) lamellar region of the eutectic at higher magnification showing the C36 phase and (d) the D810 phase.

3.2 Microstructure and mechanical properties of AX541 alloy after FSP

The microstructure of the AXM541 Mg alloy after friction stir processing in the nugget region showed extensive grain refinement compared to the base (as-cast) microstructure (Figure 3 (a)). The eutectic phase was significantly refined in the form of very fine particles (highlighted in Figure 3 (b)) dispersed homogeneously throughout the microstructure along with some larger remaining particles, as it was in the as-cast microstructure (Figure 3 (b)). An EDS scan of the

large particles revealed that they were rich in Al and Mn and may correspond to the D810 phase (Figure 3 (c)). Moreover, since unlike the C36 particles, the D810 particles remained intact and did not break down during FSP, the implication is that they must be strong and insoluble in the matrix. Figure 3 (d) indicated the presence of a mainly equi-axed grain structure after FSP in the nugget region of the AXM541 alloy, with an average grain size of 4.5 ± 0.25 μm. New, fine recrystallized grains (Figure 3 (d_1-d_4)) located primarily near the C36 particles (Figure 3 (d_1')), suggest their potential use as nucleation sites during FSP.

Figure 4 (a) confirms that the engineering stress-strain curve deformed under tensile loading for three specimens at a strain rate of 1×10^{-3} s^{-1}. They clearly indicated high tensile yield stress (TYS) of the alloy (322 ± 14 MPa). Ultimate tensile strength improved to 361 ± 17 MPa resulted in a strain hardening ability (UTS-TYS) of 39 MPa. The total elongation of 16 ± 3% (Figure 4 (a)) was significant along the processing direction. True stress-strain curve and the resultant work hardening response for Sample 3 (Figure 4 (b)) clearly show stage III work hardening operating during deformation. The continuous drop in work hardening is interrupted at a plastic strain of 3%, which points to the transition of the deformation accommodation mechanism away from the conventional slip. The hardness value of the alloy also reached an average value of 74 HV in the nugget region, as compared to the base hardness value of 53 HV (Figure 4 (c)).

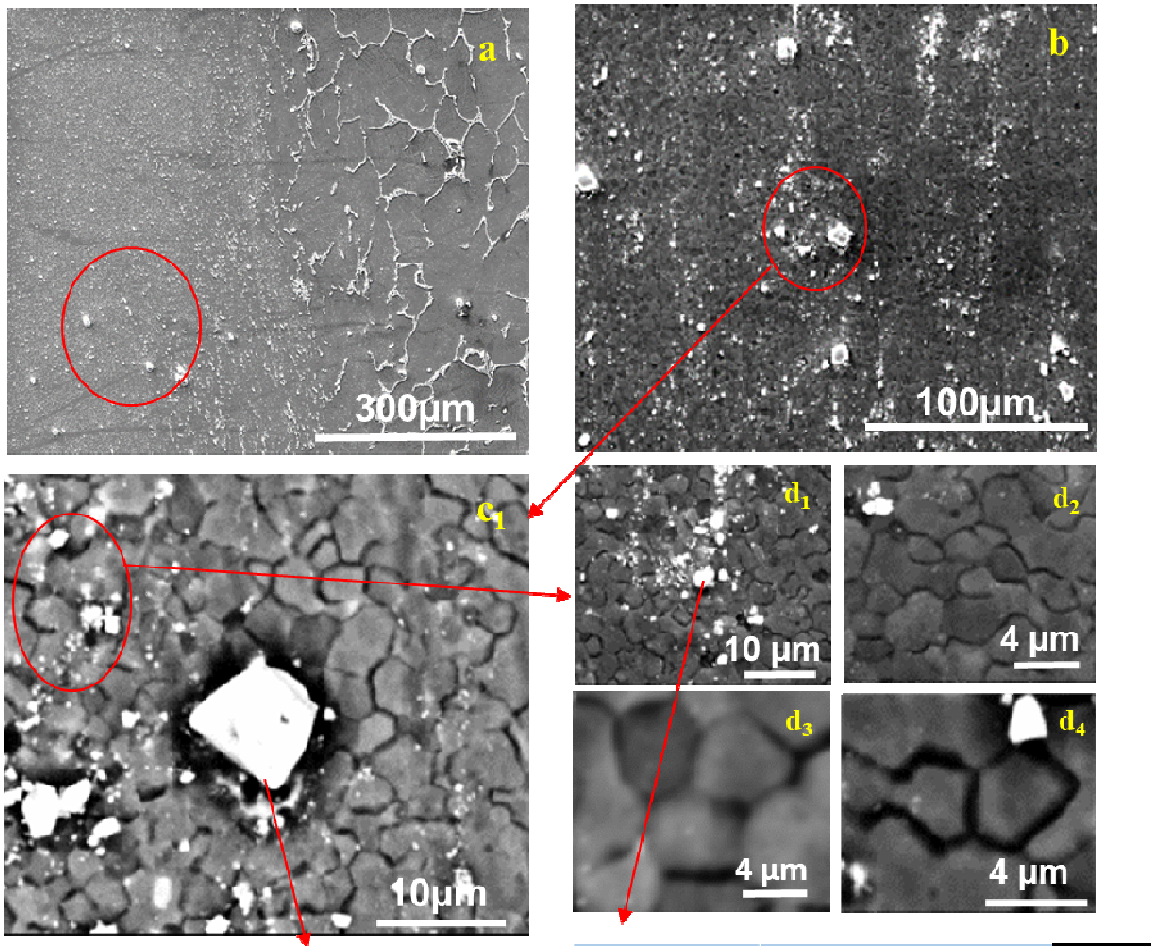

Elements	weight percentage (%)
Al	45
Mn	58

c_2

Elements	weight percentage (%)
Al	22
Ca	9

d_1'

Figure 3. Secondary electron images showing (a) friction stir processed (nugget) and base microstructure, (b) nugget microstructure displaying refined eutectic particles, (c_1 and c_2) Mn-rich particles including EDS point analysis, (d_1-d_4) polygonal grain structures and recrystallized grains near broken eutectic particles, and (d_1') EDS scans of the broken eutectic particles revealing the presence of primarily Al and Ca.

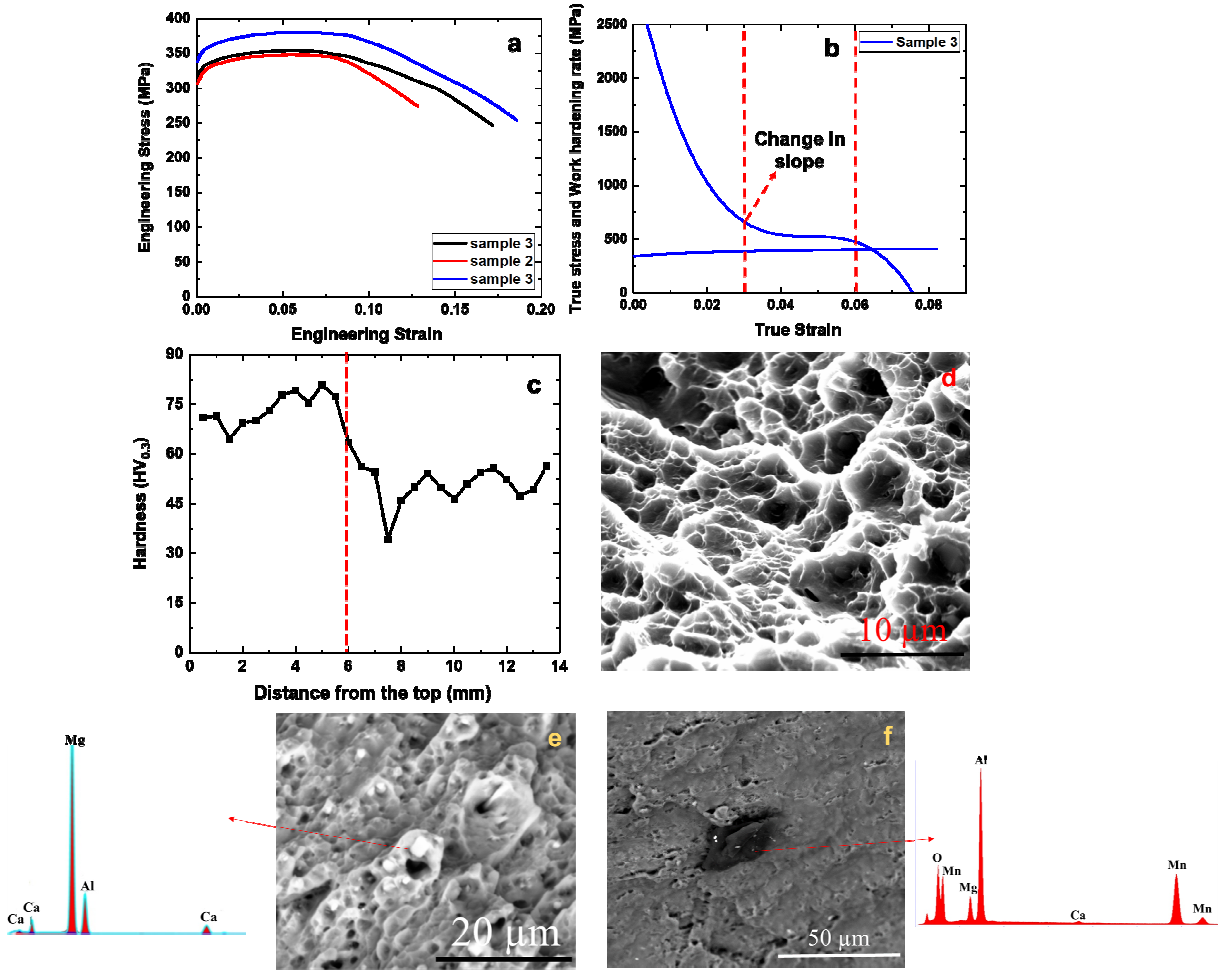

Figure 4. (a) Engineering stress-engineering strain curves, (b) true stress-true strain and work hardening curves for AXM541 alloy along the processing direction for sample 3, (c) hardness variation in nugget region, (d) fracture surface of tensile sample deformed along the processing direction and (e, f) Backscattered electron images and corresponding EDS scans showing Al-Ca- and Al-Mn-rich particles.

Table 2: Tensile properties of AXM541 alloy for as-cast and as-FSP conditions

Condition	YS (MPa)	UTS (MPa)	Elongation (%)
As-cast	125 ± 9	150 ± 13	12 ± 4
As-FSP	322 ± 14	361 ± 17	16 ± 3

As suggested by the softening (Figure 4 (a)) and by analyzing the fracture surface (Figure 4 (d)), SEM confirmed the ductile nature of the alloy. As expected, the complete dimple region in the fractograph endorsed reasonable alloy ductility. Moreover, the backscattered electron

images of the fracture surface (and their respective EDS scans) also revealed the presence of Al-Ca- and Al-Mn-rich particles. After FSP, the Al-Ca-rich particles were very fine compared to the Al-Mn-rich particles (Figure 4 (e,f)). Therefore, the larger Al-Mn-rich particles may have acted as crack nucleation sites, thus limiting overall alloy ductility.

4. Discussion

4.1 Development of ultrafine grained microstructure containing Al-Ca and Al-Mn particles upon FSP

Recent studies of the AXM series Mg alloys have focused mainly on microstructure refinement after extrusion. The addition of Al was attributed to improved ductility, whereas Ca acted as a grain refiner [9-14, 15]. Li et al. [9] explained that the effect of the Ca/Al ratio on the microstructure and its refinement was significant. They further elaborated that extrusion led to extensive grain refinement due to dynamic recrystallization assisted by particle stimulated nucleation (PSN). Very fine particles homogeneously present throughout the microstructure were either Ca-rich or Al-rich, depending on the Ca/Al ratio [9]. Lower Ca/Al ratios resulted in fine Al-rich particles, intermediate ratios led to the presence of C36 particles, and higher ratios resulted in fine Ca-rich particles. According to Al-Samman et al. [17] and Humpreus et al. [18], particle sizes larger than 1 μm assisted with PSN, as the larger particles provided higher strain gradients and higher dislocation densities locally, thereby leading to the nucleation of recrystallized grains. Thus, both Ca/Al ratio and particle size were critical for grain refinement during extrusion of the AXM Mg alloys [9-19].

Another concern was the presence of Al-Mn rich (Al_8Mn_5) compounds in the microstructure, which did not experience significant refinement during hot deformation of the AXM alloys during extrusion. Nakata et al. [13] systematically studied the effect of Mn content on the microstructure and its refinement during deformation. They reported that an increase in Mn led to a corresponding increase in the size and volume fraction of unbreakable Al-Mn particles during deformation, and an adverse effect on the microstructures and mechanical properties of the AXM alloys [13]. They further mentioned that 0.4 wt% Mn was the optimum amount for achieving the desired effect on the microstructure [13].

The present study used FSP of AXM-series Mg for microstructure refinement. The coupling effect of heat and plastic deformation during FSP resulted in severe dynamic recovery in materials having high stacking fault energies, materials such as Al. On the contrary, low stacking

fault materials such as Mg underwent dynamic recrystallization (DRX) instead of dynamic recovery during FSP [14-15, 17-23]. Thus, in the present case, DRX was the primary mechanism for the formation of fine grains after FSP. The presence of fine C36 particles assisted DRX via PSN. Most of the particles refined during FSP were larger than 1 µm (Figure 5 (a-c)), and were sufficient for use as nucleation sites during recrystallization (Figures 3 (d_1-d_4)) [14-15, 17-19]. Recrystallized grains formed near the C36 particles during FSP confirmed that PSN occurred during recrystallization (Figure 5 (a-c)). Moreover, larger Al-Mn particles were also important for PSN due to their increased size-dependent strain gradient [6, 14-15, 17-19]. That few of the D810 particles were fragmented during FSP without being severely refined indicated high shear strength. However, their presence likely enhanced DRX during FSP.

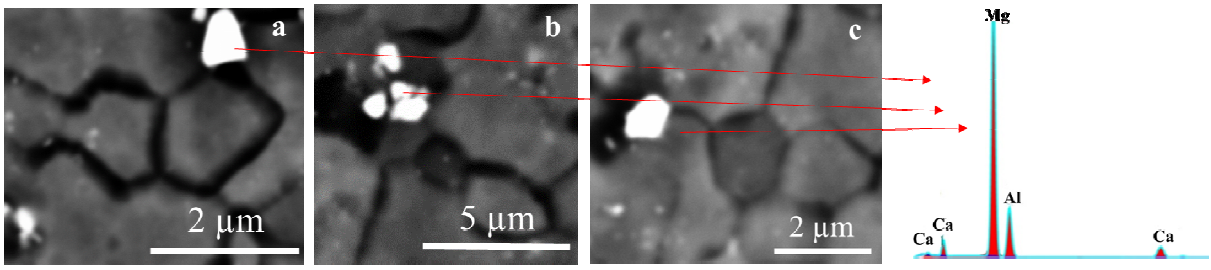

Figure 5. Secondary electron images showing fine recrystallized grains formed near the crushed C36 particles after FSP.

4.2 Stress-strain response of AXM541 alloy: comparison with leading Mg alloys

Mg alloys are associated with limited plastic accommodation at room temperature in that higher critical resolved shear stress values are required for non-basal slip to occur. As a result, extensive work has focused on enhancing the multi-slip tendency of Mg by restricting preferred grain nucleation along basal planes (i.e., (0002) basal texture) during hot deformation [1-4, 17-26]. This intended random nucleation of grains is triggered by particle stimulated nucleation (PSN), wherein intermetallic particles refined during processing act as preferential sites for the nucleation of strain-free grains, and thus result in recrystallized microstructures having grains with a variety of orientations. The addition of RE elements to Mg was a very efficient way to engineer the deformation response by altering texture evolution through PSN to trigger slip-dominant plasticity in Mg [21-23]. However, RE elements being costly make these alloys expensive for applications. Recent work on AXM series Mg alloys uses the maximum benefit of cost-effective alloying additions that promote PSN. That is, these alloys contain Mg-Al-Ca rich particles, depending on the Ca/Al ratio, which during processing gets heavily refined and thus

promotes PSN. Recent work by Sandlöbes et al. [15] showed that adding merely a very small amount of Ca to the Mg-Al system promoted the <c+a> slip during deformation and thereby resulted in good strength and ductility.

In the present study, refining and redistributing Al-Ca rich particles established a more homogenous microstructure upon FSP, which stimulated PSN and thus resulted in multi-slip dominated plasticity in the alloy. This can be further confirmed from the work hardening rate curve plotted against the plastic strain for sample 3. Figure 4 (b) makes clear that stage III of work hardening is dominant during deformation; however, a sudden change in slope in θ vs. ε plot (as marked in Figure 4 (b)) indicates the predominance of non-basal slip or twinning activity during deformation. A detailed analysis of twinning and texture evolution continues. The onset of change in slope is a strong indication of unconventional plastic deformation in the AXM541 alloy upon FSP [14-15, 17, 23-26]. Moreover, the presence of fine Al-Ca dispersoids also blocks dislocation motion and contributes to a local increase in stress required for deformation, thereby promoting sustained work hardening. In short, FSP-driven grain refinement and uniform dispersion of refined Al-Ca particles resulted in a drastic improvement in the YS to 322 ±14 MPa from the as-cast YS of ~ 125 MPa (Table 2). As mentioned in section 3.2, Al-Mn rich particles are not effectively refined during FSP and hence are suspected as crack nucleation sites during deformation (Figure 4 (f)). This hints to the possibility that the ductility of the AXM541 alloy could be improved further by manipulating the formation of Al-Mn rich particles.

Figure 6 compares YS and tensile elongation for the AXM541 alloy with other leading AXM series alloys as well as with conventional Mg alloys in a grain-refined state [9-15, 21-23]. What is apparent is either very strong AXM alloys having YS as high as 400 MPa (red square in Figure 6) with very limited plasticity; or ductile AXM alloys having very low YS (yellow downward triangle in Figure 6). Among them, the Mg-4Y-3RE alloy showed a superior combination of YS and elongation, which to-date is now outperformed by the AXM541 alloy (red circle in Figure 6) despite no RE elements being in the alloy. Thus, the AX541 alloy is a strong candidate for lightweight, more cost-effective applications. However, the properties of these alloy can be further elevated by tuning the Al and Mn content [9-13] so as to realize effective refinement of second-phase particles during FSP and even more sustained work hardening during deformation.

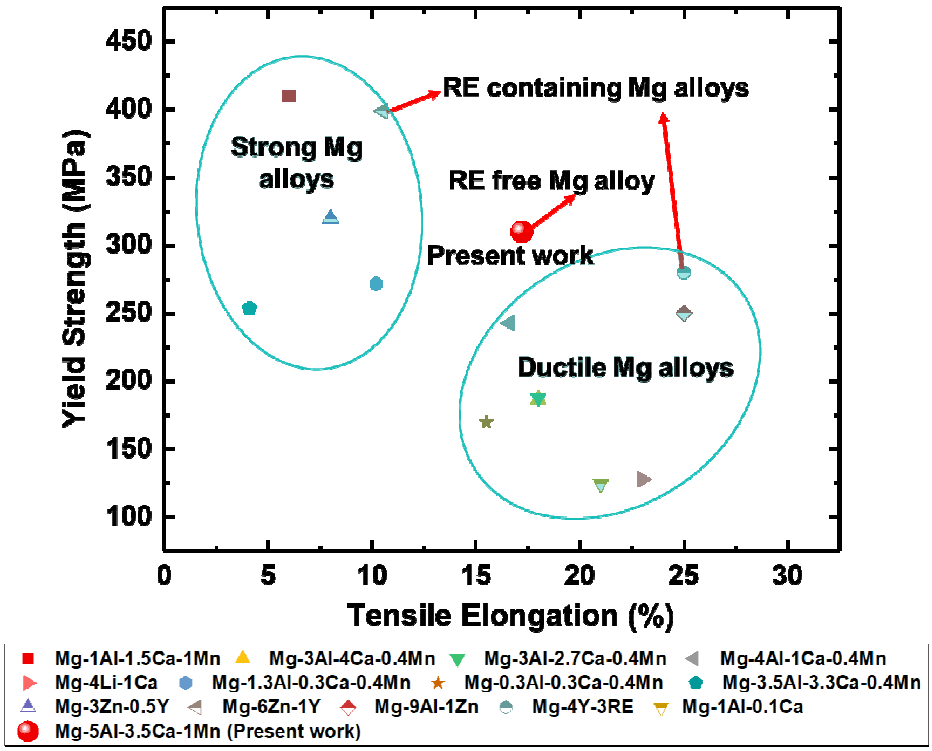

Figure 6. Yield strength and tensile elongation for AXM541 alloy and other conventional Mg alloys in grain refined condition [9-15, 21-23].

5. Conclusions

A new AXM-series Mg alloy, AXM541, was friction stir processed to obtain a fine-grained microstructure. As predicted by Thermo-Calc software, the AXM541 alloy revealed the presence of substantially refined as-cast α-Mg, αMg + $(Mg, Al)_2Ca$ eutectic (C36), and Al_8Mn_5 (D810) phases, with an average grain size of 4.5 µm after FSP. In contrast to other high Ca/Al ratio-containing AXM alloys after extrusion, the AXM541 alloy with a Ca/Al ratio of 0.7 showed high TYS values of 322 ± 14 MPa and elongation of 16 ± 3%. This severe grain refinement and the strong dispersion strengthening effect from very fine and uniformly distributed Al-Ca particles occurred after FSP triggered non-basal slip during deformation. To further improve strain hardening ability and elongation of the AXM series alloys for use in lightweight applications, the Mn/Al ratio should be tailored, since the larger Al-Mn (D810) particles experienced minimal refinement during FSP.

6. Acknowledgments

The work was performed under a cooperative agreement between the Army Research Laboratory and the University of North Texas (W911NF-13-2-0018). The authors are thankful to

the Center for Advanced Research and Technology (CART) for providing access to the microscopy facilities at the University of North Texas.

References

[1] T. Nakata, T. Mezaki, R. Ajima, C. Xu, K. Ohishi, K. Shimizu, S. Hanaki, T.T. Sasaki, K. Hono, S. Kamado, High Speed extrusion of heat treatable Mg-Al-Ca-Mn alloy, Scripta Mater. 101 (2015) 28 - 31.

[2] T. Laser, Ch. Hartig, M.R. Nu¨rnberg, D. Letzig, R. Bormann, The influence of calcium and cerium mischmetal on the microstructural evolution of Mg–3Al–1Zn during extrusion and resulting mechanical properties, Acta Mater. 56 (2008) 2791–2798.

[3] S.M. Zhu, T.B. Abbott, M.A. Gibson, J.F. Nie, M.A. Easton, Age hardening in die-cast Mg–Al–RE alloys due to minor Mn additions, Mater. Sci. Eng. A 656 (2016) 34 - 38.

[4] W.J. Kim, H.G. Jeong, H.T. Jeong, Achieving high strength and high ductility in magnesium alloys using severe plastic deformation combined with low-temperature aging, Scripta Mater. 61 (2009) 1040 -1043.

[5] S.W. Xu, N. Matsumoto, K. Yamamoto, S. Kamado, T. Honma, Y. Kojima, High temperature tensile properties of as-cast Mg–Al–Ca alloys, Mater. Sci. Eng. A 509 (2009) 105 – 110.

[6] T. Nakata, C. Xu, R. Ajima, K. Shimizu, S. Hanaki, T.T. Sasaki, L. Ma, K. Hono, S. Kamado, Strong and ductile age-hardening Mg-Al-Ca-Mn alloy that can be extruded as fast as aluminium alloys, Acta Mater. 130 (2017) 261-270.

[7] S. Xiong, F. Pan, B. Jiang, X. Li, The effects of Al-Ca compounds on grain refinement of Mg-Ca alloys, Mater. Sci. Forum 686 (2011) 348-354.

[8] B. Zhang, Y. Wang, L. Geng, C. Lu, Effect of Ca on texture and mechanical properties of hot extruded Mg-Zn-Ca alloy, Mater. Sci. Eng. A 539 (2012) 56-60.

[9] Z.T. Li, X.D. Zhang, M.Y. Zheng, X.G. Quio, K. Wu, C. Xu, S. Kamado, Effect of Ca/Al ratio on microstructure and mechanical properties of Mg-Al-Ca-Mn alloys, Mater. Sci. Eng., A 682 (2017) 423-432.

[10] F. Guo, B. Feng, S. Fu, Y. Xin, S. Xu, Q. Liu, Microstructure and texture in an extruded Mg-Al-Ca-Mn flat oval tube, J. Magnesium Alloys 5 (2017) 13-19.

[11] J. Yang, J. Peng, E.A. Nyberg, F. Pan, Effect of Ca addition on corrosion behavior of Mg-Al-Mn alloy, App. Surface Sci. 369 (2016) 92-100.

[12] S.W. Xu, K. Ohishi, S. Kamado, F. Uchida, T. Homma, K. Hono, High strength extruded Mg-Al-Ca-Mn alloy, Scripta Mater. 65 (2011) 269-272.

[13] T. Nakata, C. Xu, Y.Matsumoto, K. Shimizu, T.T. Sasaki, K. Hono, S. Kamado, Optimization of Mn content for high strengths in high speed extruded Mg-0.3Al-0.3Ca dilute alloy, Mater. Sci. Eng., A 673 (2016) 443-449.

[14] Y. Estrin, S.S. Nene, B.P. Kashyap, N. Prabhu, T. Al-Samman, New Hot Rolled Mg-4Li-1Ca alloy: A potential candidate for automotive and biodegradable implant applications. Mater Let. 173 (2016) 252-256.

[15] S. Sandlöbes, M. Friák, S. Korte-Kerzel, Z. Pei, J. Neugebauer, D. Raabe, A rare-earth free magnesium alloy with improved intrinsic ductility, Sci. Rep. 7 (2017) 10458.

[16] K.K. Sankaran, R.S. Mishra, Metallurgy and Design of Alloys with Hierarchical Microstructures, Elsevier, 2017, ISBN: 978-0-128-12068-2.

[17] T. Al-Samman, Comparative study of the deformation behavior of hexagonal magnesium–lithium alloys and a conventional magnesium AZ31 alloy, Acta Mater. 57 (2009) 2229-2242.

[18] F.J. Humphreys, M. Hatherly, Recrystallization and Related Annealing phenomena, Pergamon Press, 1996, Oxford.

[19] T. Al-Samman, G. Gottstein, Dynamic recrystallization during high temperature deformation of magnesium, Mater. Sci. Eng., A 490 (2008) 411-420.

[20] H. Y. Wang, Z. P. Yu, L. Zhang, C. G. Liu, M. Zha, C. Wang, Q. C. Jiang, Achieving high strength and high ductility in magnesium alloy using hard-plate rolling (HPR) process, Sci. Rep. 5: (2015) 17100.

[21] J. M. Rosalie, H. Somekawa, A. Singh, T. Mukai, Effect of precipitation on strength and ductility in a Mg–Zn–Y alloy, J. Alloys Compd. 550 (2013) 114-123.

[22] A. Singh, H. Somekaw, T. Mukai, High temperature processing of Mg–Zn–Y alloys containing quasicrystal phase for high strength, Mater. Sci. Eng., A 528 (2011) 6647-6651.

[23] N. Kumar, N. Dendge, R. Banerjee, R.S. Mishra, Effect of microstructure on the uniaxial tensile deformation behavior of Mg–4Y–3RE alloy, Mater. Sci Eng., A 590 (2014) 116–131.

[24] S.S. Nene, B.P. Kashyap, N. Prahu, Y. Estrin, T. Al-Samman, Microstructure refinement and its effect on specific strength and bio-corrosion resistance in ultralight Mg-4Li-1Ca (LC41) alloy by hot rolling. J. Alloys Compd. 615 (2014) 501-506.

[25] R.S. Mishra, P.S. De, N. Kumar, Friction stir welding of Magnesium alloys, in: Friction stir welding and processing: science and engineering, Springer international publishing, Switzerland, 2014, pp. 162-171.

[26] W. Yuan, R.S. Mishra, Grain size and texture effects on deformation behavior of AZ31 magnesium alloy, Mater. Sci. Eng., A 558 (2012) 716–724.